Crystal structure of ribociclib hydrogen succinate, $(C_{23}H_{31}N_8O)(HC_4H_4O_4)$

James A. Kaduk,[1,2,a] Anja Dosen,[3] and Thomas N. Blanton[3]
[1]*Illinois Institute of Technology, 3101 S. Dearborn St., Chicago, IL 60616, USA*
[2]*North Central College, 131 S. Loomis St., Naperville, IL 60540, USA*
[3]*ICDD, 12 Campus Blvd., Newtown Square, PA 19073-3273, USA*

(Received 26 January 2024; accepted 15 April 2024)

The crystal structure of ribociclib hydrogen succinate (commonly referred to as ribociclib succinate) has been solved and refined using synchrotron X-ray powder diffraction data, and optimized using density functional theory techniques. Ribociclib hydrogen succinate crystallizes in space group *P*-1 (#2) with $a = 6.52215(4)$, $b = 12.67120(16)$, $c = 18.16978(33)$ Å, $\alpha = 74.0855(8)$, $\beta = 82.0814(4)$, $\gamma = 88.6943(1)°$, $V = 1430.112(6)$ Å^3, and $Z = 2$ at 295 K. The crystal structure consists of alternating layers of cations and anions parallel to the *ab*-plane. The protonated N in each ribociclib cation acts as a donor in two strong N–H···O hydrogen bonds to two different succinate anions. Strong O–H···O hydrogen bonds link the hydrogen succinate anions into chains parallel to the *a*-axis. N–H···N hydrogen bonds link the cations into dimers, with a graph set *R2,2(8)*. The result is a three-dimensional hydrogen bond network. The powder pattern has been submitted to ICDD for inclusion in the Powder Diffraction File™ (PDF®)

[doi:10.1017/S0885715624000277]

Key words: ribociclib, Kisqali®, powder diffraction, Rietveld refinement, density functional theory

I. INTRODUCTION

Ribociclib succinate (marketed under the trade names Kisqali® and Kryxana®) is used to treat selected types of advanced or metastatic breast cancer in premenopausal or postmenopausal women. The systematic name (CAS Registry Number 1374639-75-4) is 7-cyclopentyl-*N*, *N*-dimethyl-2-[(5-piperazin-1-ylpyridin-2-yl)amino]pyrrolo [2,3-d]pyrimidine-6-carboxamide butanedioic acid. A two-dimensional molecular diagram of ribociclib hydrogen succinate is shown in Figure 1.

Ribociclib succinate is claimed, and a powder pattern is provided, in International Patent Application WO 2012/064805 A1 (Calienni et al., 2012; Novartis and Astex Therapeutics); however, a crystal structure was not reported. Novel forms of ribociclib succinate are claimed in US Patent 9,193,732 B2 (Calienni et al., 2015; Novartis and Astex Therapeutics). Crystalline forms SRS-I and SRS-II of ribociclib succinate, as well as an amorphous form, are claimed in International Patent Application WO 2019/123364 A1 (Rampalli et al., 2019; Shilpa Medicare Ltd.). Crystalline forms C-2, C-3, C-4, C-5, C-6, C-7, C-8, C-9, and C-10 are claimed in International Patent Application WO 2019/167068 A1 (Pathi et al., 2019; Cipla Ltd.). Crystalline form APO-I is claimed in US Patent 10,611,772 B2 (Souza and Khalili, 2020; Apotex). Crystalline forms M10, M11, M12, M14, and M15 are claimed in International Patent Application WO 2020/225827 (Jetti et al., 2020; Mylan Laboratories Ltd.). Novel crystalline and amorphous forms are claimed in US Patent 11,111,250 B2 (Rampalli et al., 2021; Shilpa Medicare Ltd.).

This work was carried out as part of a project (Kaduk et al., 2014) to determine the crystal structures of large-volume commercial pharmaceuticals, and include high-quality powder diffraction data for them in the Powder Diffraction File (Gates-Rector and Blanton, 2019).

II. EXPERIMENTAL

Ribociclib succinate was a commercial reagent, purchased from TargetMol (Batch #144117), and was used as-received. The white powder was packed into a 1.5 mm diameter Kapton capillary, and rotated during the measurement at ~50 Hz. The powder pattern was measured at 295 K at beamline 11-BM (Antao et al., 2008; Lee et al., 2008; Wang et al., 2008) of the Advanced Photon Source at Argonne National Laboratory using a wavelength of 0.459744(2) Å from 0.5 to 40° 2θ with a step size of 0.001° and a counting time of 0.1 s per step. The high-resolution powder diffraction data were collected using twelve silicon crystal analyzers that allow for high angular resolution, high precision, and accurate peak positions. A mixture of silicon (NIST SRM 640c) and alumina (NIST SRM 676a) standards (ratio Al_2O_3:Si = 2:1 by weight) was used to calibrate the instrument and refine the monochromatic wavelength used in the experiment.

The pattern was indexed using both N-TREOR (Altomare et al., 2013) and DICVOL14 (Louër and Boultif, 2014)

[a]Author to whom correspondence should be addressed. Electronic mail: kaduk@polycrystallography.com

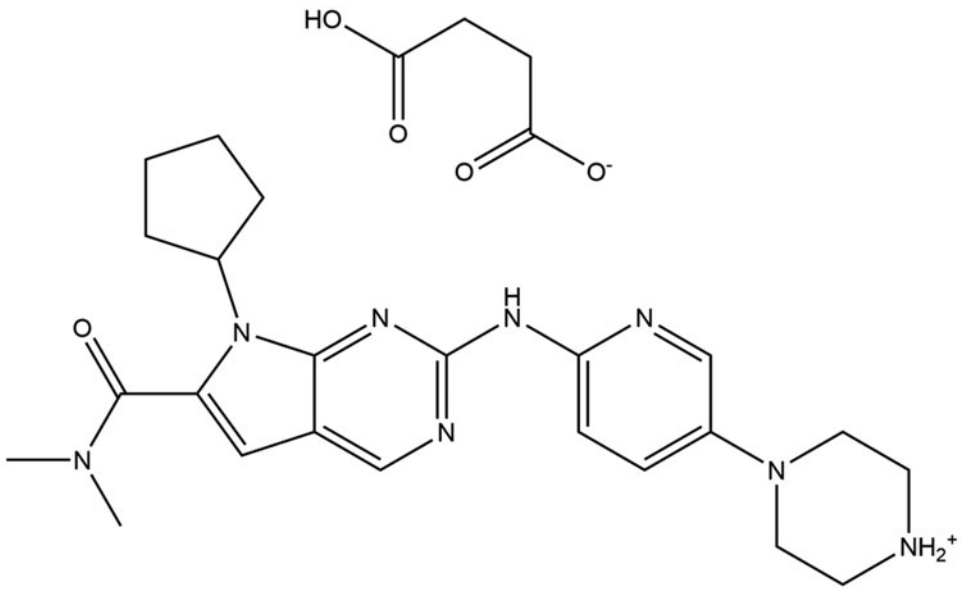

Figure 1. The two-dimensional structure of ribociclib hydrogen succinate.

through the PreDICT interface (Blanton et al., 2019) on a primitive triclinic unit cell with $a = 6.5192$, $b = 12.6781$, $c = 18.1671$ Å, $\alpha = 74.105$, $\beta = 81.996$, $\gamma = 88.675°$, $V = 1429.95$ Å^3, and $Z = 2$. The space group was assumed to be P-1, which was confirmed by successful solution and refinement of the structure. A reduced cell search of the Cambridge Structural Database (Groom et al., 2016) yielded no hits.

The ribociclib molecule was downloaded from PubChem (Kim et al., 2023) as Conformer3D_CID_44631912.sdf. It was converted to a *.mol2 file using Mercury (Macrae et al., 2020). A succinate anion was built using Spartan '20 (Wavefunction, 2022) and saved as a .mol2 file. The crystal structure was solved using Monte Carlo simulated annealing techniques as implemented in DASH (David et al., 2006), using ribociclib and succinate molecules as the fragments. Examination of close intermolecular contacts (potential hydrogen bonds) indicated that N7 and O70 were protonated, and thus, the compound is correctly named ribociclib hydrogen succinate.

Rietveld refinement was carried out with GSAS-II (Toby and Von Dreele, 2013). Only the 1.0–25.0° portion of the pattern was included in the refinements ($d_{min} = 1.062$ Å). The region 1.58–1.89° 2θ, which contained a moderately sharp peak from the Kapton capillary, was excluded. All non-H bond distances and angles were subjected to restraints, based on a Mercury/Mogul Geometry Check (Bruno et al., 2004; Sykes et al., 2011). The Mogul average and standard deviation for each quantity were used as the restraint parameters. The pyridine ring and the fused ring system were restrained to be

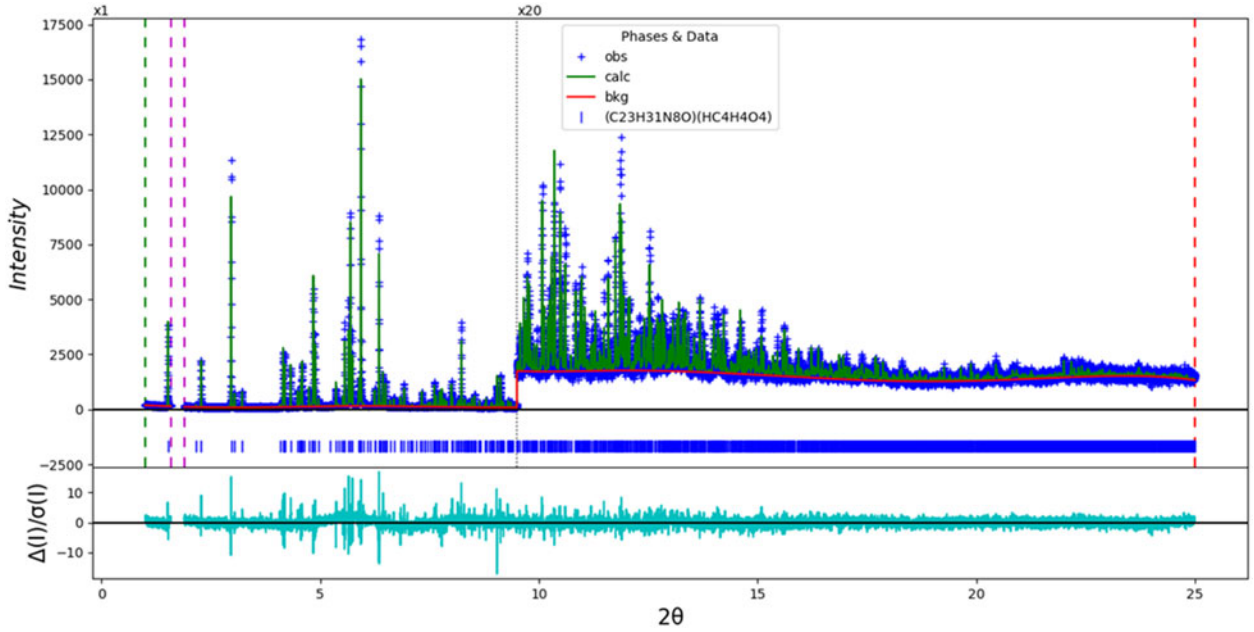

Figure 2. The Rietveld plot for the refinement of ribociclib hydrogen succinate. The blue crosses represent the observed data points, and the green line is the calculated pattern. The cyan curve is the normalized error plot, and the red line is the background curve. The vertical scale has been multiplied by a factor of 20× for $2\theta > 9.5°$.

https://doi.org/10.1017/S0885715624000277 Published online by Cambridge University Press

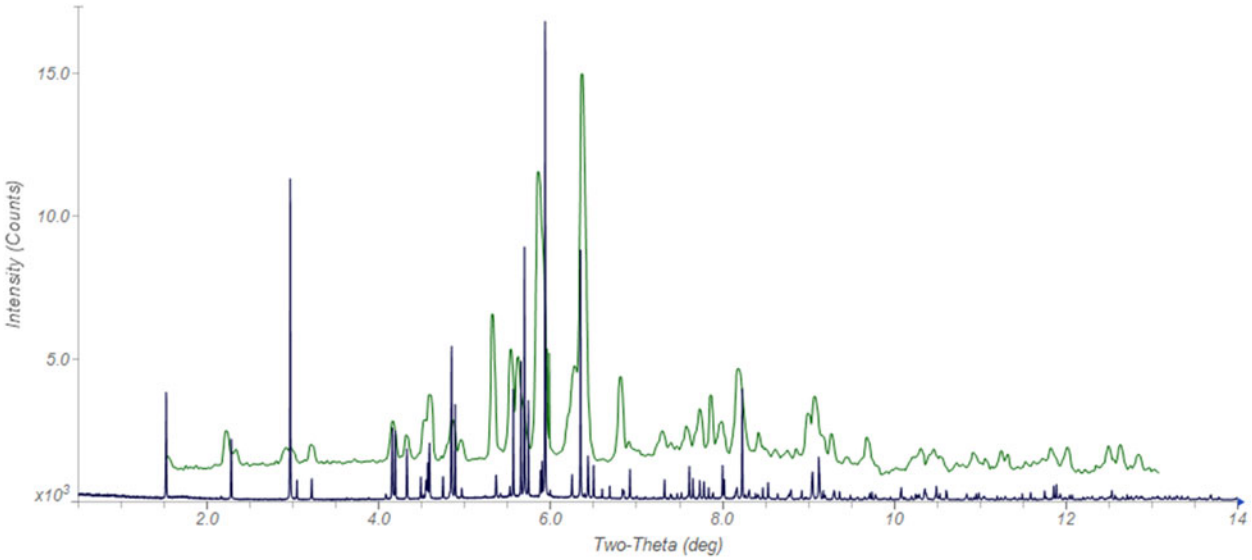

Figure 3. Comparison of the synchrotron pattern of ribociclib hydrogen succinate (black) from this study to that reported by Calienni et al. (2012; green). The literature pattern (measured using Cu K_α radiation) was digitized using UN-SCAN-IT (Silk Scientific, 2013) and converted to the synchrotron wavelength of 0.459744(2) Å using JADE Pro (MDI, 2023). Image generated using JADE Pro (MDI, 2023).

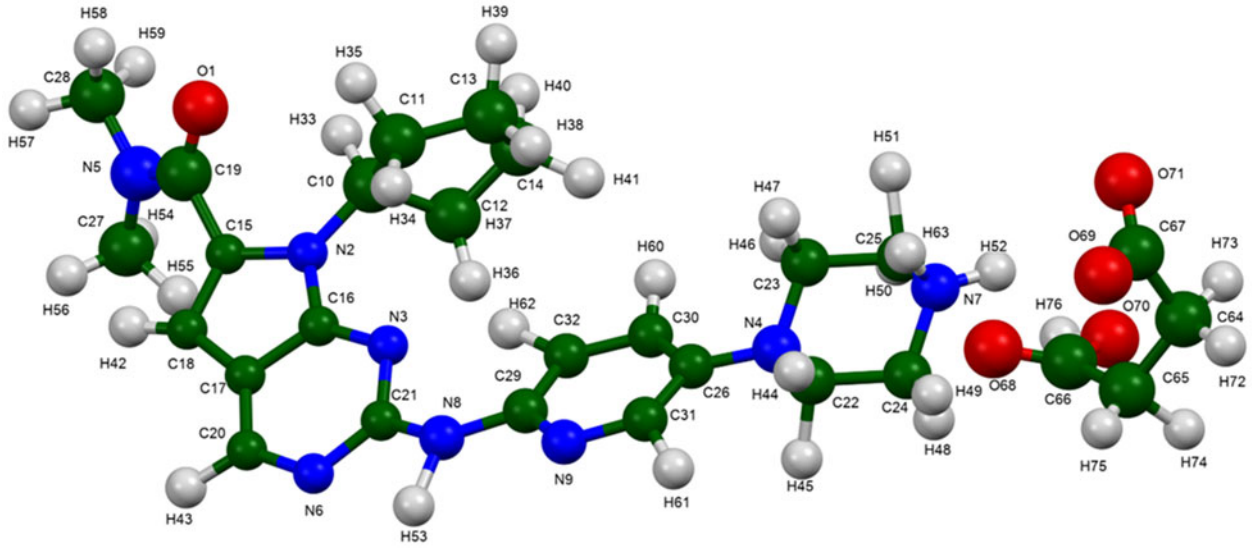

Figure 4. The asymmetric unit of ribociclib hydrogen succinate, with the atom numbering. The atoms are represented by 50% probability spheroids. Image generated using Mercury (Macrae et al., 2020).

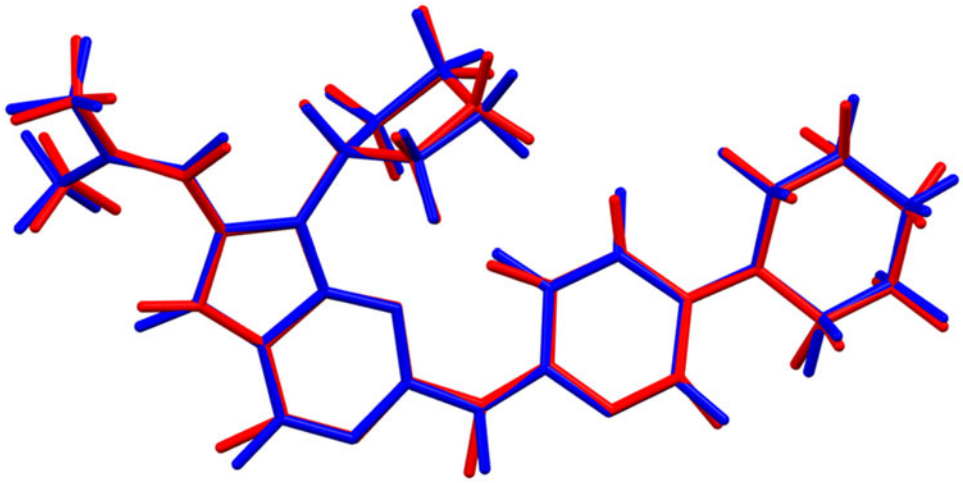

Figure 5. Comparison of the Rietveld-refined (red) and VASP-optimized (blue) structures of the ribociclib cation ribociclib hydrogen succinate. The rms Cartesian displacement is 0.088 Å. Image generated using Mercury (Macrae et al., 2020).

https://doi.org/10.1017/S0885715624000277 Published online by Cambridge University Press

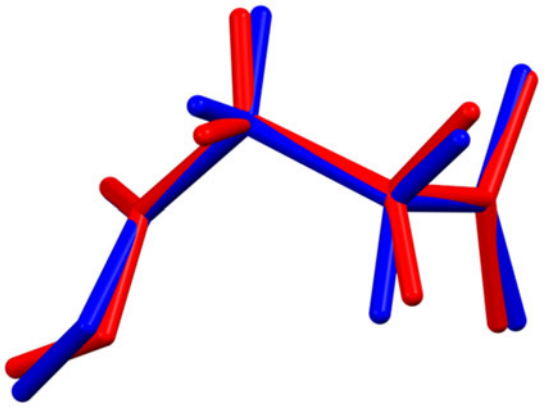

Figure 6. Comparison of the Rietveld-refined (red) and VASP-optimized (blue) structures of the hydrogen succinate anion in ribociclib hydrogen succinate. The rms Cartesian displacement is 0.102 Å. Image generated using Mercury (Macrae et al., 2020).

planar. The restraints contributed 4.1% to the final χ^2. The hydrogen atoms were included in calculated positions, which were recalculated during the refinement using Materials Studio (Dassault, 2022). The U_{iso} of the C, N, and O atoms were grouped by chemical similarity. The U_{iso} for the H atoms were fixed at 1.3× the U_{iso} of the heavy atoms to which they are attached. The peak profiles were described using a uniaxial microstrain model, with 100 as the unique axis.

The final refinement of 159 variables using 23 731 observations and 104 restraints yielded the residuals $R_{wp} = 0.12521$ and GOF = 1.52. The largest peak (0.09 Å from C10) and hole (1.61 Å from N3) in the difference Fourier map were 0.57(10) and −0.46(10) eÅ^{-3}, respectively. The final Rietveld plot is shown in Figure 2. The largest features in the normalized error plot represent a subtle error in peak shapes, the result of using a simple profile model.

The crystal structure of ribociclib hydrogen succinate was optimized (fixed experimental unit cell) with density functional techniques using VASP (Kresse and Furthmüller, 1996) through the MedeA graphical interface (Materials Design, 2016). The calculation was carried out on 16 2.4 GHz processors (each with 4 Gb RAM) of a 64-processor HP Proliant DL580 Generation 7 Linux cluster at North Central College. The calculation used the GGA-PBE functional, a plane wave cutoff energy of 400.0 eV, and a k-point spacing of 0.5 Å^{-1} leading to a 2 × 2 × 1 mesh, and took ∼8.7 h. Single-point density functional calculations (fixed experimental cell) and population analysis were carried out using CRYSTAL23 (Erba et al., 2023). The basis sets for the H, C, N, and O atoms in the calculation were those of Gatti et al. (1994). The calculations were run on a 3.5 GHz PC using 8 k-points and the B3LYP functional, and took ∼3.6 h.

III. RESULTS AND DISCUSSION

The agreement between the powder pattern of ribociclib hydrogen succinate of this study and the pattern reported by Calienni et al. (2012) is good enough to conclude that the material in this study is the same as that patented by Novartis (Figure 3). The intensities in the patent pattern differ from those observed here, probably indicating some preferred orientation and/or granularity. There are also a few weak extra peaks, perhaps indicating the presence of an impurity.

The asymmetric unit (Figure 4) contains one ribociclib cation and one hydrogen succinate anion, showing that the compound is properly described as ribociclib hydrogen succinate. The root-mean-square (rms) Cartesian displacement of

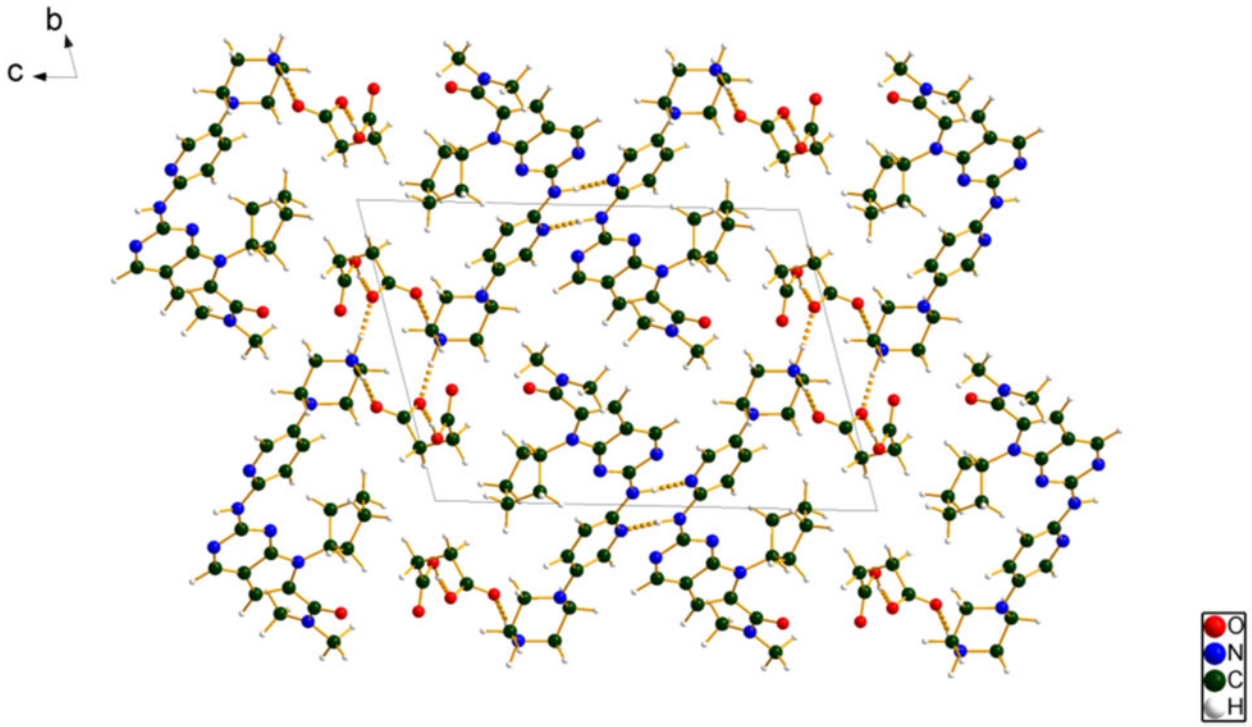

Figure 7. The crystal structure of ribociclib hydrogen succinate, viewed down the a-axis. Image generated using Diamond (Crystal Impact, 2023).

https://doi.org/10.1017/S0885715624000277 Published online by Cambridge University Press

TABLE I. Hydrogen bonds (CRYSTAL23) in ribociclib hydrogen succinate.

H-Bond	D–H (Å)	H···A (Å)	D···A (Å)	D–H···A (°)	Overlap (*e*)	*E* (kcal mol^{-1})
N7–H63···O71	1.067	1.720	2.782	173.0	0.091	7.0
N7–H52···O69	1.055	1.692	2.728	165.9	0.074	6.3
N8–H53···N9	1.047	1.896	2.942	175.3	0.078	
O70–H76···O69	1.037	1.516	2.546	172.0	0.082	15.7
C32–H62···N3	1.085	2.238[a]	2.903	117.4	0.011	
C31–H61···N6	1.092	2.328	3.267	143.0	0.025	
C30–H60···O71	1.092	2.590	3.667	168.8	0.017	
C28–H58···N4	1.097	2.901	3.951	160.5	0.011	
C27–H56···C18	1.103	2.882	3.801	140.7	0.010	
C27–H55···C15	1.094	2.529[a]	2.953	101.7	0.014	
C25–H50···O68	1.100	2.278	3.363	168.5	0.029	
C23–H46···O71	1.095	2.210	3.268	161.6	0.029	
C13–H39···O70	1.098	2.556	3.456	138.5	0.012	
C10–H33···O1	1.094	2.205[a]	2.933	121.7	0.010	
C65–H75···O69	1.097	2.676[a]	3.005	96.5	0.010	

[a]Intramolecular.

the non-H atoms in the Rietveld-refined and VASP-optimized cation is 0.088 Å (Figure 5) and in the succinate anion is 0.102 Å (Figure 6). The agreement is within the normal range for correct structures (van de Streek and Neumann, 2014), and provides confirmation that the structure is correct. The remainder of this discussion will emphasize the VASP-optimized structure.

Almost all of the bond distances, bond angles, and torsion angles fall within the normal ranges indicated by a Mercury/Mogul Geometry check (Macrae et al., 2020). The torsion angles involving rotation about the C65–C66 bond in the succinate anion are flagged as unusual. They lie on long tails of peaked distributions, and indicate that the succinate anion conformation is unusual.

Quantum chemical geometry optimization of the isolated cation (DFT/B3LYP/6-31G*/water) using Spartan '20 (Wavefunction, 2022) indicated that the solid-state conformation is 6.6 kcal mol^{-1} higher in energy than a local minimum, which is the global minimum-energy conformation. A similar optimization indicated that the solid-state conformation of the anion is 6.0 kcal mol^{-1} higher in energy than a local minimum, which has different orientations of the carboxyl groups. The global minimum-energy conformation of the anion has a similar backbone, but again different orientations of the carboxyl groups. Apparently, the hydrogen bonding affects the solid-state conformation.

The crystal structure (Figure 7) consists of alternating layers of cations and anions parallel to the *ab*-plane. As discussed below, hydrogen bonding is important in the structure. Analysis of the contributions to the total crystal energy of the structure using the Forcite module of Materials Studio (Dassault Systèmes, 2022) suggests that angle distortion terms are the most important contributors to the intramolecular energy, as expected from a fused ring system. The intermolecular energy is dominated by electrostatic attractions, which in the force-field analysis include hydrogen bonds. The hydrogen bonds are better analyzed using the results of the DFT calculation.

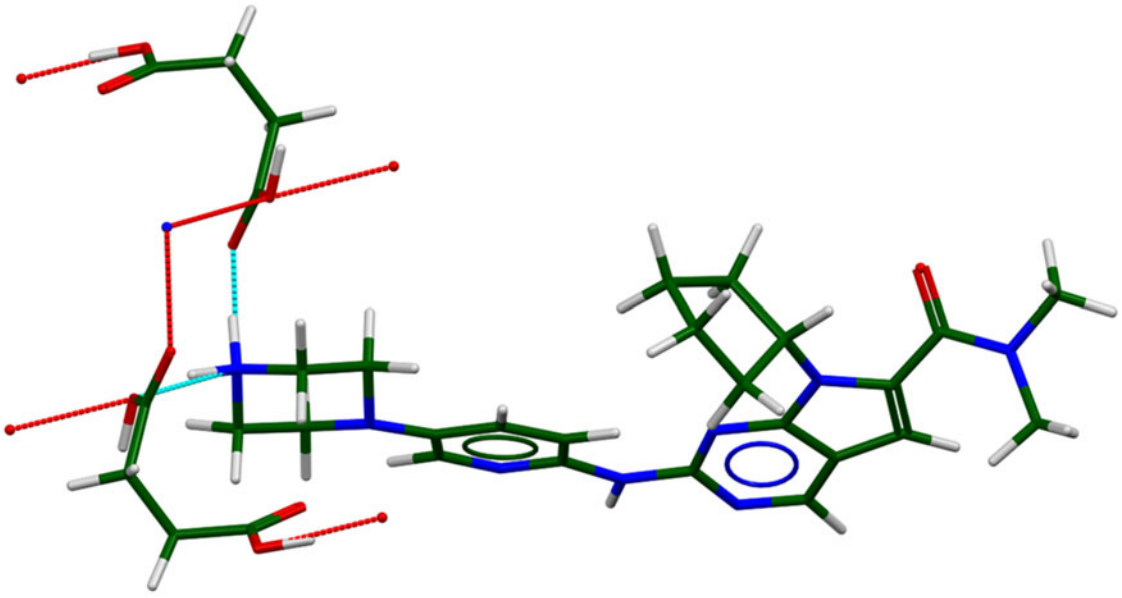

Figure 8. The hydrogen bonds (light blue dotted lines) of the ribociclib cation connect to two succinate anions. The dotted red lines indicate other hydrogen bonds. Image generated using Mercury (Macrae et al., 2020).

https://doi.org/10.1017/S0885715624000277 Published online by Cambridge University Press

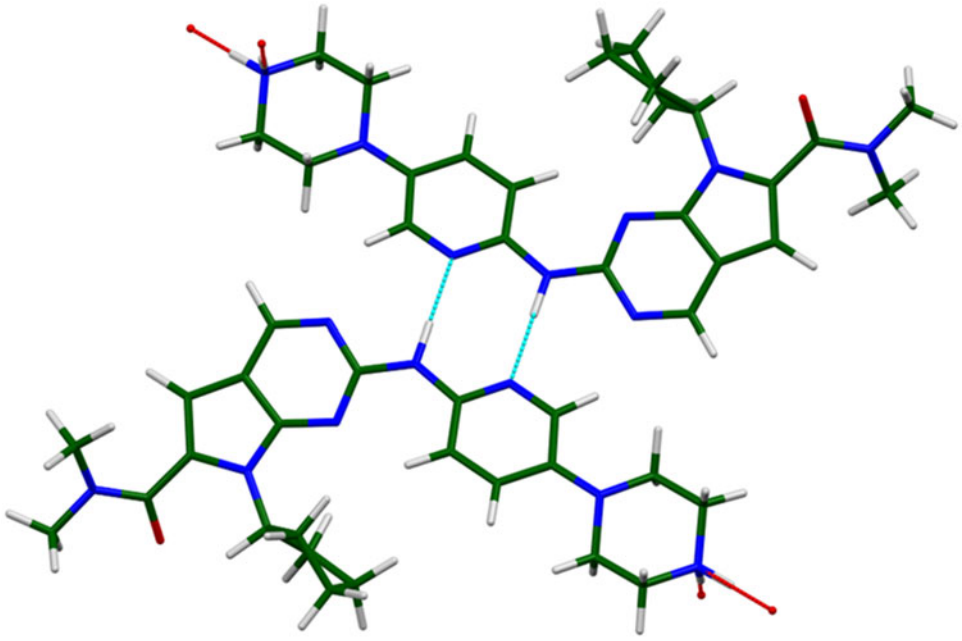

Figure 9. The hydrogen-bonded dimer of ribociclib cations (light blue lines). The dark red dotted lines indicate cation–anion hydrogen bonds. Image generated using Mercury (Macrae et al., 2020).

Hydrogen bonds (Table I) are important in the structure. The protonated N7 in each ribociclib acts as a donor in two strong N–H···O hydrogen bonds to two different succinate anions (Figure 8). Strong O–H···O hydrogen bonds link the hydrogen succinate anions into chains parallel to the *a*-axis. N–H···N hydrogen bonds link the cations into dimers, with a graph set (Etter, 1990; Bernstein et al., 1995; Shields et al., 2000) *R2,2(8)* (Figure 9). The result is a three-dimensional hydrogen bond network. The energies of the O–H···O hydrogen bonds were calculated using the correlation of Rammohan and Kaduk (2018), and those of the N–H···O hydrogen bonds using the correlation of Wheatley and Kaduk (2019). A variety of C–H···O, C–H···N, and C–H···C hydrogen bonds link the cations and anions, also contributing to the lattice energy.

The volume enclosed by the Hirshfeld surface of ribociclib hydrogen succinate (Figure 10; Hirshfeld, 1977; Spackman et al., 2021) is 704.73 Å^3, 98.55% of the unit cell volume. The packing density is thus fairly typical. The only significant close contacts (red in Figure 10) involve the hydrogen bonds. The volume/non-hydrogen atom is typical, at 17.9 Å^3.

The Bravais–Friedel–Donnay–Harker (Bravais, 1866; Friedel, 1907; Donnay and Harker, 1937) morphology suggests that we might expect elongated morphology for ribociclib hydrogen succinate, with <100> as the long axis, or platy morphology with {001} as the major faces. A fourth-order spherical harmonic model was included in the refinement. The texture index was 1.0066(1), indicating that the preferred orientation was not significant in this rotated capillary specimen.

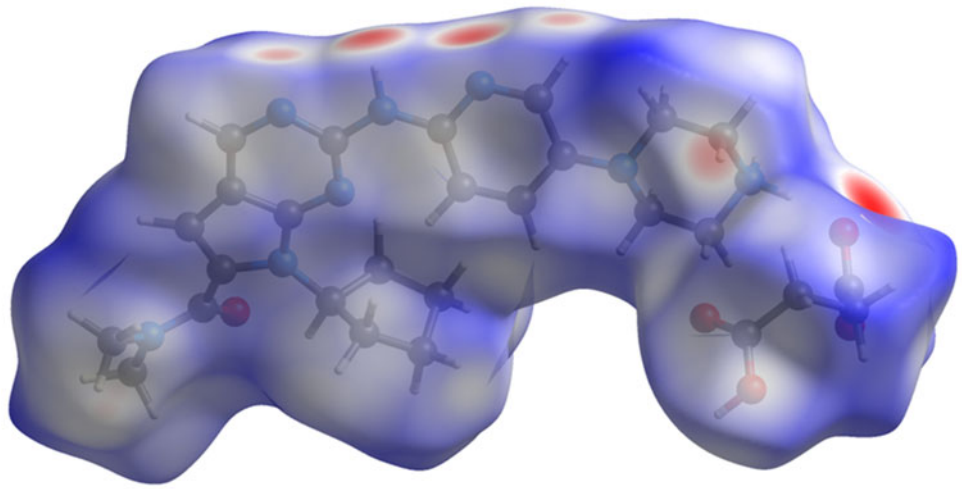

Figure 10. The Hirshfeld surface of ribociclib hydrogen succinate. Intermolecular contacts longer than the sums of the van der Waals radii are colored blue, and contacts shorter than the sums of the radii are colored red. Contacts equal to the sums of radii are white. Image generated using CrystalExplorer (Spackman et al., 2021).

https://doi.org/10.1017/S0885715624000277 Published online by Cambridge University Press

IV. DEPOSITED DATA

The powder pattern of ribociclib hydrogen succinate from this synchrotron data set has been submitted to ICDD for inclusion in the Powder Diffraction File. The Crystallographic Information Framework (CIF) files containing the results of the Rietveld refinement (including the raw data) and the DFT geometry optimization were deposited with the ICDD. The data can be requested at pdj@icdd.com

ACKNOWLEDGMENTS

The use of the Advanced Photon Source at Argonne National Laboratory was supported by the U.S. Department of Energy, Office of Science, Office of Basic Energy Sciences, under Contract No. DE-AC02-06CH11357. This work was partially supported by the International Centre for Diffraction Data. We thank Saul Lapidus for his assistance in the data collection.

CONFLICTS OF INTEREST

The authors have no conflicts of interest to declare.

REFERENCES

Altomare, A., C. Cuocci, C. Giacovazzo, A. Moliterni, R. Rizzi, N. Corriero, and A. Falcicchio. 2013. "EXPO2013: A Kit of Tools for Phasing Crystal Structures from Powder Data." *Journal of Applied Crystallography* 46: 1231–35.

Antao, S. M., I. Hassan, J. Wang, P. L. Lee, and B. H. Toby. 2008. "State-of-the-Art High-Resolution Powder X-ray Diffraction (HRPXRD) Illustrated with Rietveld Refinement of Quartz, Sodalite, Tremolite, and Meionite." *Canadian Mineralogist* 46: 1501–9.

Bernstein, J., R. E. Davis, L. Shimoni, and N. L. Chang. 1995. "Patterns in Hydrogen Bonding: Functionality and Graph Set Analysis in Crystals." *Angewandte Chemie International Edition in English* 34: 1555–73.

Blanton, J., R. Papoular, and D. Louër. 2019. "PreDICT: A Graphical User Interface to the DICVOL14 Indexing Software Program for Powder Diffraction Data." *Powder Diffraction* 34: 233–41.

Bravais, A. 1866. *Etudes Cristallographiques*. Paris: Gauthier Villars.

Bruno, I. J., J. C. Cole, M. Kessler, J. Luo, W. D. S. Motherwell, L. H. Purkis, B. R. Smith, R. Taylor, R. I. Cooper, S. E. Harris, and A. G. Orpen. 2004. "Retrieval of Crystallographically-Derived Molecular Geometry Information." *Journal of Chemical Information and Computer Sciences* 44: 2133–44.

Calienni, J. V., G.-P. Chen, B. Gong, P. K. Kapa, & V. Saxena. 2012. "Salt(s) of 7-cyclopentyl-2-(5-piperazin-1-yl-pyridin-2-ylamino)-7H-pyrrlo [2,3-D]pyrimidine-6-carboxylic acid dimethylamide and process of making thereof." International Patent Application WO 2012/064805 A1.

Calienni, J. V., G.-P. Chen, B. Gong, P. K. Kapa, & V. Saxena. 2015. "Salt(s) of 7-cyclopentyl-2-(5-piperazin-1-yl-pyridin-2-ylamino)-7H-pyrrlo [2,3-D]pyrimidine-6-carboxylic acid dimethylamide and process of making thereof." United States Patent 9,193,732 B2.

Crystal Impact. 2023. Diamond. V. 5.0.0. Crystal Impact - Dr. H. Putz & Dr. K. Brandenburg. Windows.

Dassault Systèmes. 2022. *Materials Studio 2023*. San Diego, CA: BIOVIA.

David, W. I. F., K. Shankland, J. van de Streek, E. Pidcock, W. D. S. Motherwell, and J. C. Cole. 2006. "DASH: A Program for Crystal Structure Determination from Powder Diffraction Data." *Journal of Applied Crystallography* 39: 910–15.

Donnay, J. D. H., and D. Harker. 1937. "A New Law of Crystal Morphology Extending the Law of Bravais." *American Mineralogist* 22: 446–47.

Erba, A., J. K. Desmarais, S. Casassa, B. Civalleri, L. Donà, I. J. Bush, B. Searle, L. Maschio, L.-E. Daga, A. Cossard, C. Ribaldone, E. Ascrizzi, N. L. Marana, J.-P. Flament, and B. Kirtman. 2023. "CRYSTAL23: A Program for Computational Solid State Physics and Chemistry." *Journal of Chemical Theory and Computation* 19: 6891–932. doi:10.1021/acs.jctc.2c00958.

Etter, M. C. 1990. "Encoding and Decoding Hydrogen-Bond Patterns of Organic Compounds." *Accounts of Chemical Research* 23: 120–26.

Friedel, G. 1907. "Etudes sur la loi de Bravais." *Bulletin de la Société Française de Minéralogie* 30: 326–455.

Gates-Rector, S., and T. N. Blanton. 2019. "The Powder Diffraction File: A Quality Materials Characterization Database." *Powder Diffraction* 39: 352–60.

Gatti, C., V. R. Saunders, and C. Roetti. 1994. "Crystal-Field Effects on the Topological Properties of the Electron-Density in Molecular Crystals - The Case of Urea." *Journal of Chemical Physics* 101: 10686–96.

Groom, C. R., I. J. Bruno, M. P. Lightfoot, and S. C. Ward. 2016. "The Cambridge Structural Database." *Acta Crystallographica Section B: Structural Science, Crystal Engineering and Materials* 72: 171–79.

Hirshfeld, F. L. 1977. "Bonded-Atom Fragments for Describing Molecular Charge Densities." *Theoretica Chemica Acta* 44: 129–38.

Jetti, R. R., D. Bhatraju, R. M. R. Golivi, S. R. Manukonda, S. Jayachandra, & C. Khanduri. 2020. "Novel Polymorphs of Ribociclib Succinate." International Patent Application WO 2020/225827 A1.

Kaduk, J. A., C. E. Crowder, K. Zhong, T. G. Fawcett, and M. R. Suchomel. 2014. "Crystal Structure of Atomoxetine Hydrochloride (Strattera), $C_{17}H_{22}NOCl$." *Powder Diffraction* 29: 269–73.

Kim, S., J. Chen, T. Cheng, A. Gindulyte, J. He, S. He, Q. Li, B. A. Shoemaker, P. A. Thiessen, B. Yu, L. Zaslavsky, J. Zhang, and E. E. Bolton. 2023. "PubChem 2023 Update." *Nucleic Acids Research* 51 (D1): D1373–80. doi:10.1093/nar/gkac956.

Kresse, G., and J. Furthmüller. 1996. "Efficiency of Ab-Initio Total Energy Calculations for Metals and Semiconductors Using a Plane-Wave Basis Set." *Computational Materials Science* 6: 15–50.

Lee, P. L., D. Shu, M. Ramanathan, C. Preissner, J. Wang, M. A. Beno, R. B. Von Dreele, L. Ribaud, C. Kurtz, S. M. Antao, X. Jiao, and B. H. Toby. 2008. "A Twelve-Analyzer Detector System for High-Resolution Powder Diffraction." *Journal of Synchrotron Radiation* 15: 427–32.

Louër, D., and A. Boultif. 2014. "Some Further Considerations in Powder Diffraction Pattern Indexing with the Dichotomy Method." *Powder Diffraction* 29: S7–S12.

Macrae, C. F., I. Sovago, S. J. Cottrell, P. T. A. Galek, P. McCabe, E. Pidcock, M. Platings, G. P. Shields, J. S. Stevens, M. Towler, and P. A. Wood. 2020. "*Mercury 4.0*: From Visualization to Design and Prediction." *Journal of Applied Crystallography* 53: 226–35.

Materials Design. 2016. *MedeA 2.20.4*. Angel Fire, NM, Materials Design Inc.

MDI. 2023. *JADE Pro Version 8.3*. Livermore, CA, Materials Data.

Pathi, S. L., D. R. Rao, G. Malhotra, R. Chennuru, M. Bollineni, S. Ashwathanarayana, V. S. Pullela, & A. Mithun. 2019. "Novel Polymorphs of Ribociclib Succinate." International Patent Application WO 2019/167068 A1.

Rammohan, A., and J. A. Kaduk. 2018. "Crystal Structures of Alkali Metal (Group 1) Citrate Salts." *Acta Crystallographica Section B: Crystal Engineering and Materials* 74: 239–52. doi:10.1107/S2052520618002330.

Rampalli, S., L. K. Upalla, S. Cherukuvada, C. B. Needi, G. K. Dasari, & V. M. M. R. Seshagiri. 2019. "Novel Polymorphs of Ribociclib Mono Succinate." International Patent Application WO 2019/123364 A1.

Rampalli, S., L. K. Upalla, S. Cherukuvada, C. B. Patneedi, G. K. Dasari, & V. M. M. Seshagiri. 2021. "Polymorphs of Ribociclib Mono Succinate." United States Patent 11,111,250 B2.

Shields, G. P., P. R. Raithby, F. H. Allen, and W. D. S. Motherwell. 2000. "The Assignment and Validation of Metal Oxidation States in the Cambridge structural Database." *Acta Crystallographica Section B: Structural Science* 56: 455–65.

Silk Scientific. 2013. *UN-SCAN-IT 7.0*. Orem, UT, Silk Scientific Corporation.

Souza, F. E. S., and B. Khalili. 2020. "Crystalline Form of Ribociclib Succinate." United States Patent 10,611,772 B2.

Spackman, P. R., M. J. Turner, J. J. McKinnon, S. K. Wolff, D. J. Grimwood, D. Jayatilaka, and M. A. Spackman. 2021. "Crystalexplorer: A Program for Hirshfeld Surface Analysis, Visualization and Quantitative Analysis of Molecular Crystals." *Journal of Applied Crystallography* 54: 1006–11. doi:10.1107/S1600576721002910.

Sykes, R. A., P. McCabe, F. H. Allen, G. M. Battle, I. J. Bruno, and P. A. Wood. 2011. "New Software for Statistical Analysis of Cambridge

Structural Database Data." *Journal of Applied Crystallography* 44: 882–86.

Toby, B. H., and R. B. Von Dreele. 2013. "GSAS II: The Genesis of a Modern Open Source All Purpose Crystallography Software Package." *Journal of Applied Crystallography* 46: 544–49.

van de Streek, J., and M. A. Neumann. 2014. "Validation of Molecular Crystal Structures from Powder Diffraction Data with Dispersion-Corrected Density Functional Theory (DFT-D)." *Acta Crystallographica Section B: Structural Science, Crystal Engineering and Materials* 70: 1020–32.

Wang, J., B. H. Toby, P. L. Lee, L. Ribaud, S. M. Antao, C. Kurtz, M. Ramanathan, R. B. Von Dreele, and M. A. Beno. 2008. "A Dedicated Powder Diffraction Beamline at the Advanced Photon Source: Commissioning and Early Operational Results." *Review of Scientific Instruments* 79: 085105.

Wavefunction, Inc. 2022. *Spartan '20. V. 1.1.4*. Irvine, CA, Wavefunction Inc.

Wheatley, A. M., and J. A. Kaduk. 2019. "Crystal Structures of Ammonium Citrates." *Powder Diffraction* 34: 35–43.

https://doi.org/10.1017/S0885715624000277 Published online by Cambridge University Press